Journal of Fluorescence (2019) 29:451–459
https://doi.org/10.1007/s10895-019-02355-7

ORIGINAL ARTICLE

An Imidazo[1,5-α]Pyridine-Based Fluorometric Chemodosimeter for the Highly Selective Detection of Hypochlorite in Aqueous Media

Suh Mi Hwang [1] · Dongju Yun [1] · Cheal Kim [1]

Received: 2 November 2018 / Accepted: 25 January 2019 / Published online: 2 February 2019

Abstract

A new fluorometric chemodosimeter 2-amino-3-(((*E*)-3-(1-phenylimidazo[1,5-α]pyridin-3-yl)benzylidene)amino)maleonitrile (**BPI-MAL**) has been designed and synthesized for sensing hypochlorite. **BPI-MAL** showed a selective turn-on fluorescence for ClO^- through hypochlorite-promoted de-diaminomaleonitrile reaction. It also could detect ClO^- in the presence of various competitive anions including reactive oxygen species. Interestingly, sensor **BPI-MAL** was successfully applied as a fluorescent test kit for ClO^- determination. The sensing property and mechanism of **BPI-MAL** toward ClO^- were studied by fluorescence and UV-vis spectroscopy, NMR titration and DFT calculations.

Keywords Hypochlorite · Fluorescent chemodosimeter · Imidazo[1,5-a]pyridine · Test kit · Theoretical calculations

Introduction

Research on probes for recognition of biologically significant anions has drawn huge interest in chemosensing field [1–9]. Hypochlorous acid, one of ROS (reactive oxygen species), is known as a microbicidal mediator in human immune defense system [10–13]. It is formed from the reaction of Cl^- and H_2O_2 catalyzed by MPO (myeloperoxidase) to destroy the invasive bacteria and pathogens [14–17]. However, abnormal concentration of ClO^- could induce various diseases such as cancer, arthritis and Parkinson's disease [18–21]. On the other hand, ClO^-, as a strong oxidizer, is also widely employed in organic synthesis, household bleach and disinfectant with a high concentration (10^{-5}–10^{-2} M) in water treatment [22]. Considering the various usages of ClO^-, the development of accessible and selective tools to sense ClO^- is of high importance.

Recently, various analytical methods including colorimetric, fluorescent, chemiluminescence and electrochemical have been developed to detect ClO^- [23–36]. Among these methods, fluorescent methods are considered as an effective way to detect ClO^- owing to their short response time, high sensitivity and accurate analysis [37–40]. In this respect, several fluorescent probes including various fluorophores have been developed to recognize ClO^- like pyrene, BODIPY, coumarin and fluorescein [24, 29, 41–43]. In addition, fluorescent probes which react with ClO^- through covalent interaction could enhance selectivity as a ClO^- sensor. With the points in mind, we synthesized a chemodosimeter **BPI-MAL** bearing a new type fluorescent **BPI** and diaminomaleonitrile. **BPI-MAL** acted as a reaction-based fluorescent chemosensor for ClO^- through the production of the fluorescent aldehyde **BPI**.

Herein, we report a new chemodosimeter **BPI-MAL** for sensing ClO^- by turn-on fluorescence. **BPI-MAL** displayed a strong greenish blue fluorescence upon selective reaction with ClO^-. Importantly, the sensor clearly recognized ClO^- in the presence of ROS species (H_2O_2, AcOOH and *t*BuOOH). **BPI-MAL** was also applied to test kit experiments for the practical and rapid determination of ClO^-. Reaction mechanism and sensing process toward ClO^- were demonstrated by theoretical calculations, fluorescence, and UV-vis and ^1H NMR titrations.

Experiments

Materials and Equipment

All materials were purchased from Sigma-Aldrich. ^{13}C and ^1H NMR data were recorded on a Varian spectrometer. UV-

Electronic supplementary material The online version of this article (https://doi.org/10.1007/s10895-019-02355-7) contains supplementary material, which is available to authorized users.

✉ Cheal Kim
chealkim@seoultech.ac.kr

[1] Department of Fine Chemistry, Seoul National University of Science and Technology, Seoul 129-743, South Korea

visible and fluorescence measurements were carried out with Perkin Elmer UV/Visible and LS45 fluorescent spectrometers. The fluorescent quantum yields were obtained with quinine sulfate as a standard.

Synthetic Method of 4-(1-Phenylimidazo[1,5-a] Pyridin-3-Yl)Benzaldehyde (BPI)

2-Benzoylpyridine (3.0 mmol, 0.55 g) and $NH_4(OAc)$ (15.0 mmol, 1.15 g) were dissolved in 17 mL of CH_3COOH, and isophthalaldehyde (6.3 mmol, 0.84 g) was added into the mixture. After it was refluxed about 5 h at 90 °C, acetic acid was evaporated and the resulting crude product was extracted with dichloromethane/aqueous $NaCO_3$ solution. The dichloromethane layer was collected and purified through chromatography (43:5:2, CH_2Cl_2-hexane-MeOH) to give a yellow solid (57%). ^{1}H NMR in DMSO-d_6, δ: 10.14 (s, 1H), 8.58 (d, J = 8.0 Hz, 1H), 8.41 (s, 1H), 8.24 (d, J = 8.0 Hz, 1H), 7.98 (d, J = 8.0 Hz, 3H), 7.68 (t, J = 8.0 Hz, 1H), 7.48 (t, J = 8.0 Hz, 2H), 7.30 (t, J = 8.0 Hz, 1H), 7.00 (t, J = 8.0 Hz, 1H), 6.82 (t, J = 8.0 Hz, 1H).

Synthetic Method of BPI-MAL

BPI (0.9 mmol, 270 mg) and diaminomaleonitrile (0.85 mmol, 92 mg) were dissolved in distilled EtOH (15 mL) and the mixture was refluxed about 4 h at 70 °C. A deep yellow solid was precipitated and collected by filtration with a yield of 89%. ^{1}H NMR in DMSO-d_6, δ: 8.50 (m, 2H), 8.43 (d, J = 8.0 Hz, 1H), 8.19 (d, J = 8.0 Hz, 1H), 8.02 (m, 3H), 7.97 (d, J = 8.0 Hz, 3H), 7.68 (t, J = 8.0 Hz, 1H), 7.48 (t, J = 8.0 Hz, 2H), 7.30 (t, J = 8.0 Hz, 1H), 7.00 (t, J = 8.0 Hz, 1H), 6.82 (t, J = 8.0 Hz, 1H). ^{13}C NMR (100 MHz, 25 C) d 155.16, 137.21, 136.66, 135.05, 131.61, 130.95, 130.80, 129.92, 129.40, 129.15, 129.14, 128.69, 127.90, 127.77, 126.76, 126.50, 126.45, 123.16, 121.57, 118.95, 114.80, 114.29, 114.25, 102.89. LRMS (ESI): calcd for [**BPI-MAL** - H^+ + $2H_2O$]$^-$: 423.16 (m/z), found, 423.24 (m/z).

Selectivity of BPI-MAL

2.0 mL of DMF was used to dissolve **BPI-MAL** (1.2 mg, 6 × 10^{-3} mmol). 10.0 μL (3 × 10^{-3} M) of the **BPI-MAL** solution was diluted to a mixture (2.99 mL) of PBS buffer/DMF (8:2; *v*/v) to make 10 μM. 4.2 μL (100 mM) of a number of oxidants and anions (H_2O_2, AcOOH, *t*BuOOH, Br^-, CN^-, Cl^-, $H_2PO_4^-$, NO_2^-, OAc^-, BzO^-, N_3^- and F^-) was added to 3.0 mL of **BPI-MAL** (10 μM) to produce 14 equiv. Their fluorescent data were obtained, after reacting them for 30 s.

Fluorescent and UV-Visible Titrations

2.0 mL of DMF was used to dissolve **BPI-MAL** (1.2 mg, 6 × 10^{-3} mmol). 10.0 μL (3 × 10^{-3} M) of the **BPI-MAL** solution was diluted to a mixture (2.99 mL) of PBS buffer/DMF (8:2; *v*/v) to make 10 μM. Distilled water (5 mL) was used to dilute NaClO solution (256 μL, 5 mmol). Then, 0.3–4.5 μL (or 0.3–7.8 μL for UV-visible titration) of the ClO^- were added to each solution of **BPI-MAL**. Their UV-visible and fluorescent data were obtained, after reacting them for 30 s.

^{1}H NMR Titration

To two NMR tubes of **BPI-MAL** (1.6 mg, 2 × 10^{-5} mol) dissolved in dimethylformamide-d_7 (1.4 mL) were added two different equivalents (0 and 9.0) of NaClO dissolved in D_2O (0.6 mL). After 1 min, the ^{1}H NMR spectra were recorded.

Competition Tests

4.2 μL (100 mM) of a stock ClO^- was diluted in 2.982 mL of a mixture of PBS buffer/DMF (*v*/v, 8:2). 4.2 μL (100 mM) of a number of oxidants and anions (H_2O_2, AcOOH, *t*BuOOH, Br^-, CN^-, Cl^-, $H_2PO_4^-$, NO_2^-, OAc^-, BzO^-, N_3^- and F^-) was added to ClO^- solution to produce 14 equiv. 10.0 μL (3 × 10^{-3} M) of **BPI-MAL** solution was added into each mixture of guest analytes to make 0.01 mM. Their fluorescent data were obtained, after reacting them for 30 s.

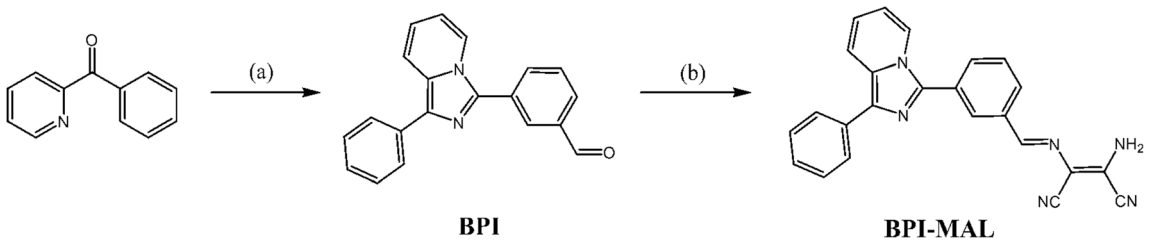

Scheme 1 Synthetic procedure of chemodosimeter **BPI-MAL**. Reagents and conditions: **a** isophthalaldehyde, ammonium acetate, acetic acid, reflux, 5 h; **b** diaminomaleonitrile, distilled EtOH, reflux, 4 h (see the experimental section for details)

pH Test

To check the pH effect on **BPI-MAL** and **BPI-MAL** + ClO^-, a series of Britton-Robinson buffer/DMF (8:2; *v*/v) having pH range from 2 to 12 were prepared. 10.0 μL (3×10^{-3} M) of a stock **BPI-MAL** solution dissolved in DMF was diluted to 2.99 mL of each pH buffer solution to afford 0.01 mM. 4.2 μL (0.1 M) of a stock ClO^- was transferred to **BPI-MAL** solution (3 mL). Their fluorescent data were obtained, after reacting them for 30 s.

Fluorescence Test Kit

A stock solution (500 μM) of **BPI-MAL** dissolved in acetonitrile was prepared. Then, filter papers were immersed into the solution of **BPI-MAL** and dried in air. Test kits coated with **BPI-MAL** were treated with 5 mM of various oxidants and anions (H_2O_2, AcOOH, *t*BuOOH, Br^-, CN^-, Cl^-, $H_2PO_4^-$, NO_2^-, OAc^-, BzO^-, N_3^- and F^-). After 30 s, the photograph of each test strip was taken under the UV light.

Theoretical Calculations

All theoretical calculations were carried out with Gaussian 03 [44]. With the hybrid functional B3LYP/6-31G(d,p) level, the geometry optimizations calculations were performed for **BPI-MAL** and **BPI** [45–48]. Imaginary frequency was not observed for the optimized forms of **BPI-MAL** and **BPI**, indicating their local minima. For all calculations, the Barone and Cossi's CPCM was used to consider the solvent effect and water was chosen as the solvent [49, 50]. CAM-B3LYP functional was applied in TD-DFT to study the electronic characters of singlet excited states at the ground state structures of **BPI-MAL** and **BPI** [51]. 30 singlet-singlet excitations were considered for calculations. The MO contributions of electronic transitions were analyzed by using GaussSum 2.1 [52].

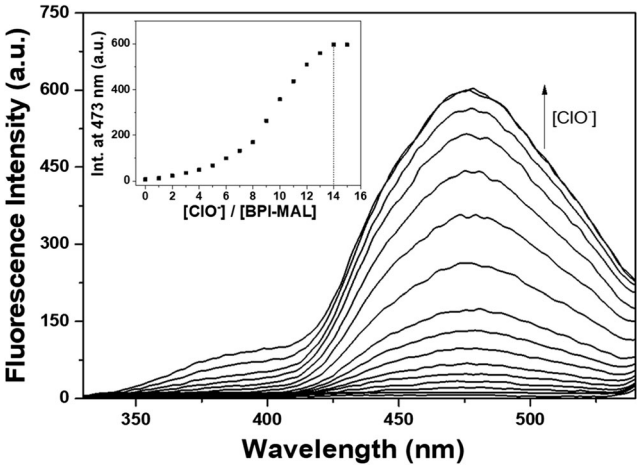

Fig. 2 Fluorescence changes of **BPI-MAL** (1×10^{-2} mM) with increasing concentrations of ClO^-. Inset: Plot of fluorescent intensity (473 nm) vs. the amount of ClO^-

Results and Discussion

Chemodosimeter **BPI-MAL** was synthesized by refluxing 4-(1-phenylimidazo[1,5-a]pyridin-3-yl)benzaldehyde (**BPI**) with diaminomaleonitrile in distilled EtOH (Scheme 1). Compound **BPI** was synthesized by

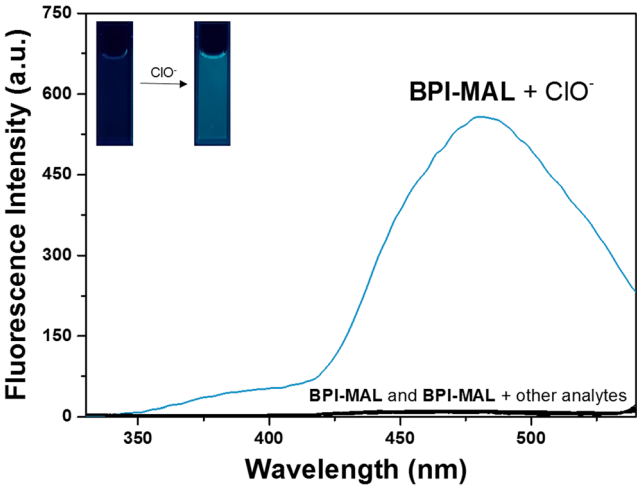

Fig. 1 Fluorescence spectra of **BPI-MAL** (1×10^{-2} mM) upon addition of various analytes (14 equiv). Inset: Fluorescent color change of **BPI-MAL** with ClO^-

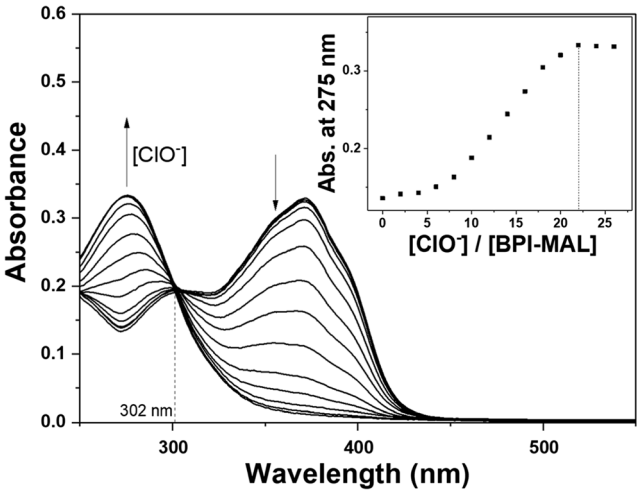

Fig. 3 UV-vis changes of **BPI-MAL** (1×10^{-2} mM) with increasing concentrations of ClO^-. Inset: Plot of absorbance (275 nm) vs. the concentration of ClO^-

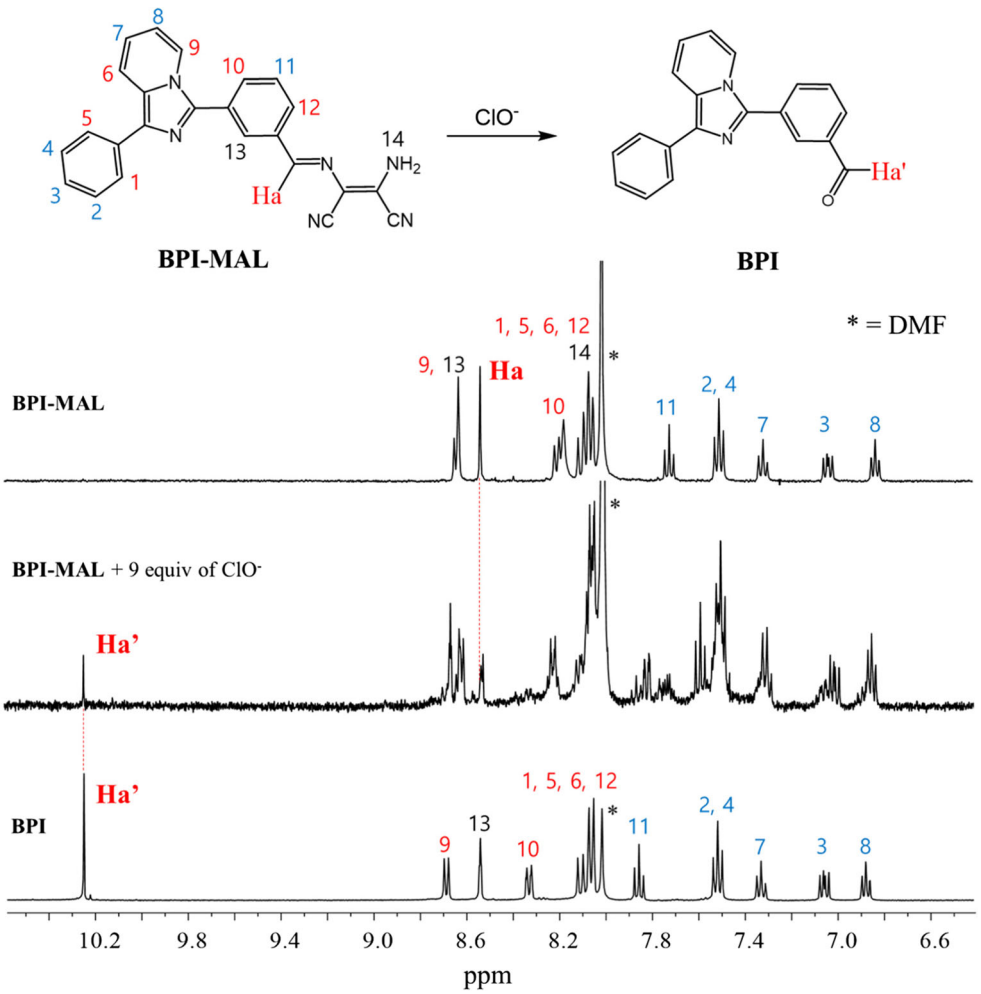

Fig. 4 ^{1}H NMR spectra of **BPI-MAL**, **BPI-MAL** + 9 equiv. of ClO^{-}, and **BPI**

condensation reaction of 2-benzoylpyridine and isophthalaldehyde. **BPI-MAL** and **BPI** were successfully characterized by ^{1}H and ^{13}C NMR and ESI-MS. In addition, the fluorescence of **BPI-MAL** was stable for 24 h in a mixture of PBS buffer/DMF (*v*/v, 8:2) (Fig. S1).

Spectroscopic Investigations of Chemodosimeter BPI-MAL to ClO^{-}

To check the selectivity, fluorescent response of **BPI-MAL** toward various guest analytes (H_2O_2, AcOOH, *t*BuOOH,

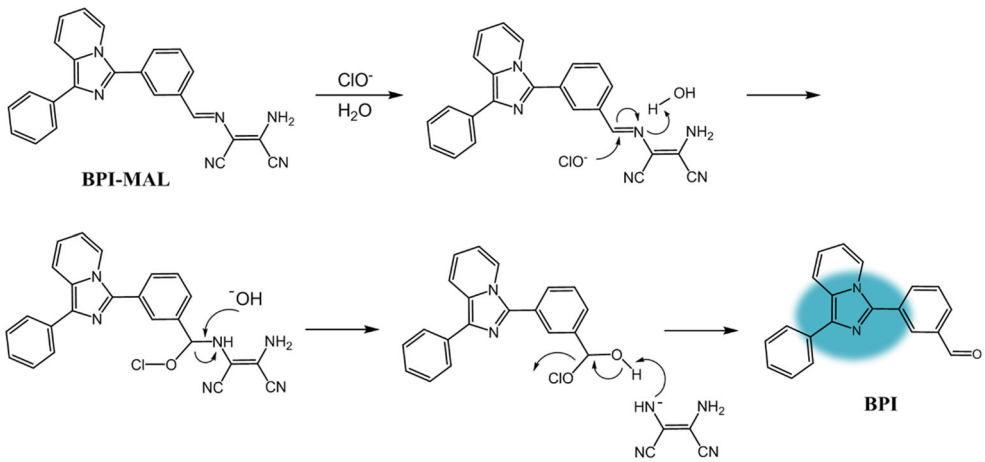

Scheme 2 Plausible sensing mechanism of ClO^{-} by **BPI-MAL**

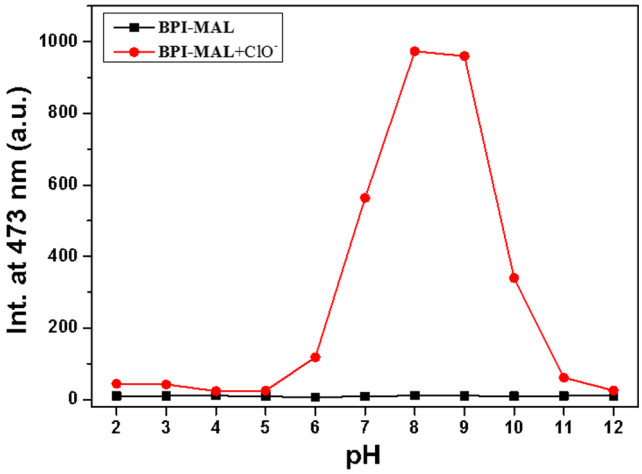

Fig. 5 Fluorescent intensity (473 nm) of **BPI-MAL** with ClO^- at pH values of 2 to 12

Br^-, CN^-, Cl^-, $H_2PO_4^-$, NO_2^-, OAc^-, BzO^-, N_3^- and F^-) were examined in PBS buffer/DMF (80:20) (Fig. 1). **BPI-MAL** displayed little fluorescence emission with a quantum yield $\Phi = 0.0056$ ($\lambda_{ex} = 275$ nm). When **BPI-MAL** was treated with 14 equiv. of the guest analytes, only ClO^- led to the remarkable fluorescence enhancement with a high quantum yield ($\Phi = 0.1230$). These results indicated that chemodosimeter **BPI-MAL** could be used as a selective fluorescent ClO^- sensor.

The chemosensing property of **BPI-MAL** toward ClO^- was investigated by fluorescence titration (Fig. 2). As different concentration of ClO^- was added into the solution of **BPI-MAL**, emission peak at 473 nm was continuously increased until ClO^- reached at 14 equiv. UV-vis titration was also conducted to further study the photophysical properties of **BPI-MAL** to ClO^- (Fig. 3). The absorbance at 275 nm increased and the band at 370 nm continuously decreased with a large hypsochromic shift (95 nm), and a defined isosbestic point appeared at 302 nm. To analyze the quantitative sensing ability of **BPI-MAL** toward ClO^-, a calibration curve was constructed in the range of 0–30 μM and a good linearity was observed ($R^2 = 0.9923$, Fig. S2). Detection limit turned out to be 2.32 μM through the IUPAC method ($C_{DL} = 3\sigma/k$) [53].

To understand the reaction mechanism of **BPI-MAL** with ClO^-, we conducted ^1H NMR titration experiment (Fig. 4). On addition of ClO^- (9 equiv) into **BPI-MAL**, the proton signal of Ha (8.55 ppm) of the imine group decreased and a new proton Ha' of the aldehyde group of **BPI** appeared at 10.25 ppm. Based on these results and literatures related to ClO^--promoted dediaminomaleonitrile reaction [54, 55], we proposed that the imine group of **BPI-MAL** was attacked by oxidizer ClO^-, resulting in the generation of corresponding aldehyde **BPI** (Scheme 2). In particular, **BPI-MAL** could detect ClO^- in the second highest water percent among previously reported ClO^- sensors that attacked the imine group to produce the cleft product aldehyde (Table S1).

To examine the practical sensing capability of **BPI-MAL** as a proper fluorescent chemodosimeter for ClO^-, the competitive tests were performed (Fig. S3). When chemodosimeter **BPI-MAL** was mixed with both competitive guest analytes (14 equiv) and ClO^- (14 equiv), most of the analytes including ROS did not inhibit the sensing of ClO^- by **BPI-MAL**. However, the presence of CN^- exhibited significant inhibition with recognizing ClO^-.

To evaluate the practical applicability of **BPI-MAL**, pH effect on the fluorescent recognition of ClO^- was studied at the range of pH 2 to 12 (Fig. 5). **BPI-MAL** showed a negligible fluorescence intensity in the whole pH range, suggesting that **BPI-MAL** is unresponsive to pH change. When **BPI-MAL** was treated with 14 equiv. of ClO^-, intensity change was not observed under acidic and hard basic conditions. However, notable increase of fluorescent intensity was observed at the range of pH 7–10. These results demonstrated that the ideal range of sensing ClO^- by probe **BPI-MAL** was between pH 7 and 10.

To check the practical application of **BPI-MAL**, test kits experiment was performed using the filter papers coated with **BPI-MAL** (Fig. 6). When the test kits were

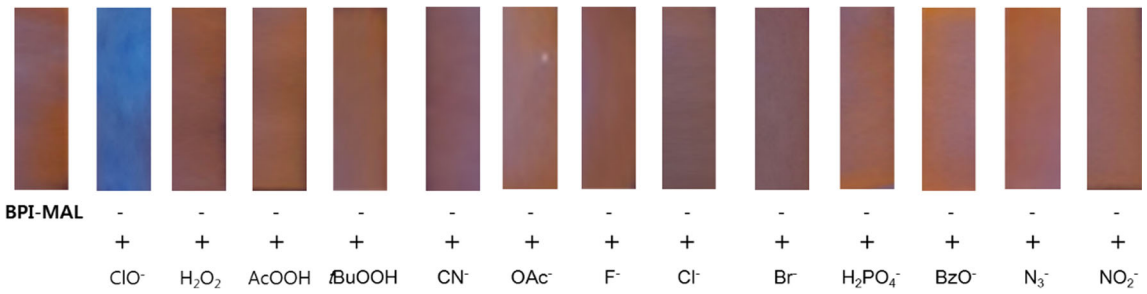

Fig. 6 Photos of the filter papers coated with **BPI-MAL** and various analytes

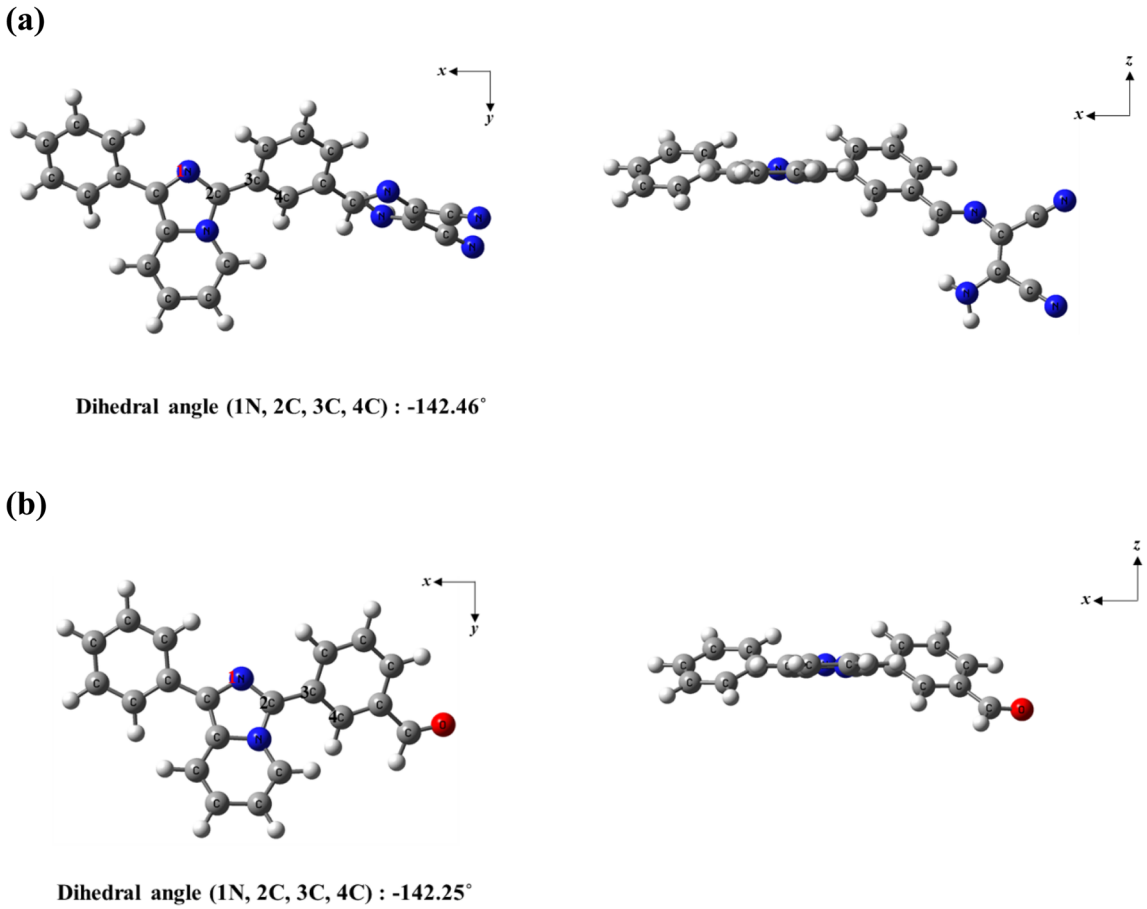

Fig. 7 Energy-minimized forms of (**a**) **BPI-MAL** and (**b**) **BPI**

treated with oxidants and anions, blue fluorescence was observed only with ClO^- under the UV light. These results suggested that the test kits coated with **BPI-MAL** can be used for detection of ClO^- in an easy and rapid way.

Calculations

To get the structural information on **BPI-MAL** and **BPI**, theoretical calculations were performed based on the experimental results. The energy-minimized structures of the two compounds were analyzed at the DFT/B3LYP/6-31G (d,p) level (Fig. 7). The structure of **BPI-MAL** had a twisted form having the dihedral angle of −142.46° (1 N, 2C, 3C, 4C) (Fig. 7a), and **BPI** showed a similar structure to **BPI-MAL** except for elimination of diaminomaleonitrile group (the dihedral angle = −142.25° for 1 N, 2C, 3C, 4C) (Fig. 7b).

To get understanding into the absorptions to the singlet excited states for **BPI-MAL** and **BPI**, CAM-B3LYP functional was applied in TD-DFT calculations and all calculations were carried out with the optimized forms. Transition energies and oscillator strengths of two compounds were shown in Figs. 8, S4, and S5. The MOs of **BPI-MAL** were calculated to be the HOMO-1 → LUMO (6.24 eV) and HOMO → LUMO transitions at the second lowest excited state (5.085 eV, 346.91 nm, Fig. S4). The HOMO-1 → LUMO excitation showed $\pi \rightarrow \pi^*$ transition. Electron density of **BPI-MAL** in both HOMO-1 and LUMO was mainly localized in diaminomaleonitrile group. The HOMO → LUMO transition was analyzed to be ICT (intramolecular charge transfer) transition, showing transfer of electron density from the imidazo[1,5-α]pyridine group to the diaminomaleonitrile one. With **BPI**, the main MO contribution was calculated to be HOMO → LUMO+3 transition at the 5th lowest excited state (7.188 eV, 266.95 nm, Fig. S5). The transition was assigned to be $\pi \rightarrow \pi^*$ transition. Electron density of both HOMO and LUMO was localized in imidazo[1,5-α]pyridine moiety. Moreover, increased energy gap of **BPI** was corresponded with the hypochromic shift of the UV-vis spectra. These results led us to propose that as a result of cleavage of diaminomaleonitrile group in **BPI-MAL**, predominant $\pi \rightarrow \pi^*$ transition in fluorophore **BPI** induced the enhancement of fluorescence emission.

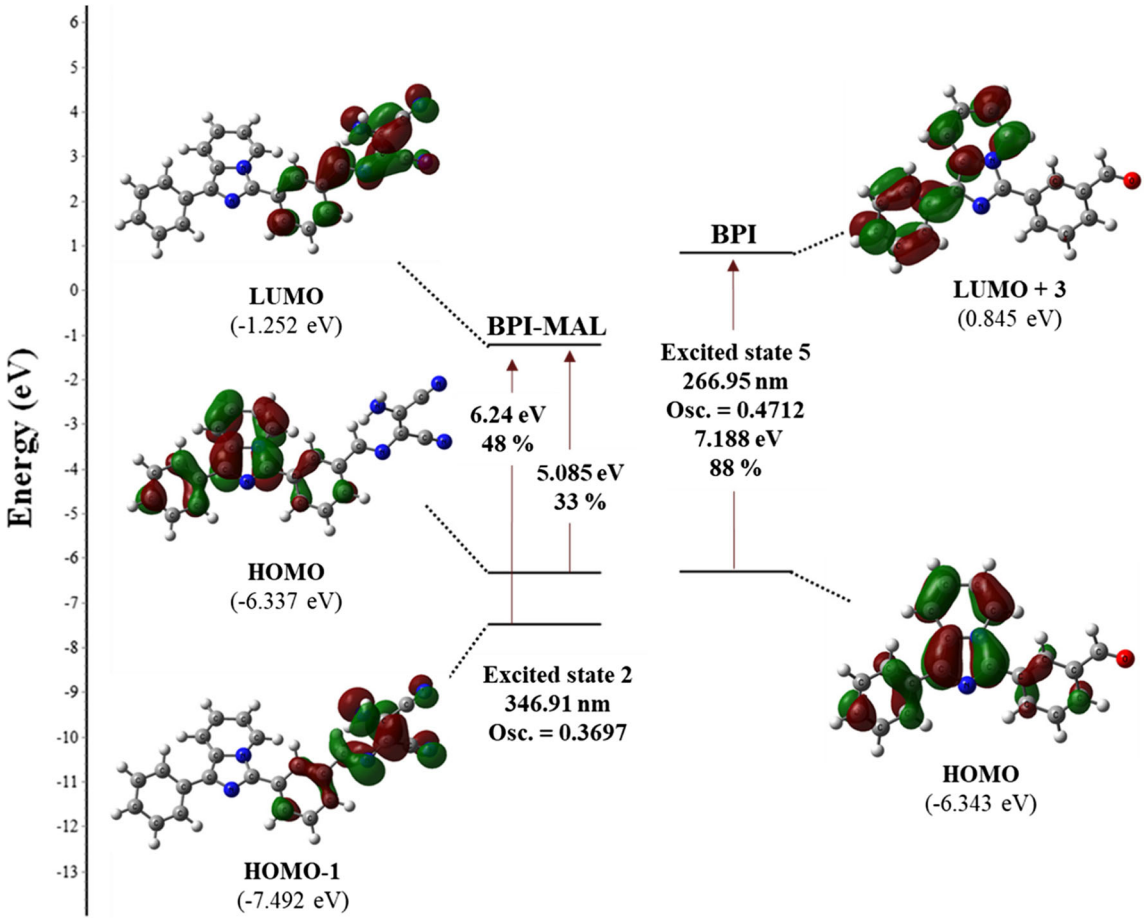

Fig. 8 MO diagrams and excitation energies of **BPI-MAL** and **BPI**

Conclusion

We presented an imidazo[1,5-α]pyridine-based fluorescent chemodosimeter **BPI-MAL** for the selective sensing of ClO^-. **BPI-MAL** alone displayed no fluorescence, whereas the fluorescence intensity with high quantum yield (22 folds) was significantly enhanced upon the addition of ClO^-. **BPI-MAL** selectively reacted with ClO^- over the various analytes including ROS, through de-diaminomaleonitrile reaction. Moreover, test kit experiment was successfully performed using **BPI-MAL**-coated filter paper for practical use. The sensing property of **BPI-MAL** toward ClO^- was illustrated by fluorescence and UV-vis spectroscopy and ^1H NMR titrations. The mechanism of ClO^--induced fluorescence behavior was further explained by DFT calculations. Thus, we expect that these results will contribute to the design and development of novel fluorescent chemodosimeters for sensing ClO^-.

Acknowledgements National Research Foundation of Korea and Korea Environment Industry & Technology Institute (NRF-2018R1A2B6001686 and KEITI-2016001970001) kindly supported this work.

References

1. Busschaert N, Caltagirone C, Van Rossom W, Gale PA (2015) Applications of supramolecular anion recognition. Chem Rev 115:8038–8155
2. Lee SY, Kim C (2016) A colorimetric chemosensor for sulfide in a near-perfect aqueous solution: practical application using a test kit. RSC Adv 6:85091–85099
3. Goswami S, Paul S, Manna A (2013) Carbazole based hemicyanine dye for both "naked eye" and 'NIR' fluorescence detection of CN^- in aqueous solution: from molecules to low cost devices (TLC plate sticks). Dalton Trans 42:10682–10686
4. Kim SK, Lee DH, Hong JI, Yoon J (2009) Chemosensors for pyrophosphate. Acc Chem Res 42:23–31
5. Chen S, Li H, Hou P (2018) A novel imidazo[1,5-α]pyridine-based fluorescent probe with a large stokes shift for imaging hydrogen sulfide. Sensors Actuators B Chem 256:1086–1092
6. Yuan Y, Zhang CJ, Xu S, Liu B (2016) A self-reporting AIE probe with a built-in singlet oxygen sensor for targeted photodynamic ablation of cancer cells. Chem Sci 7:1862–1866
7. Jeong HY, Lee SY, Kim C (2017) Furan and Julolidine-based "turn-on" fluorescence Chemosensor for detection of F^- in a near-perfect aqueous solution. J Fluoresc 27:1457–1466
8. Liu Y, Lee D, Wu D, Swamy KMK, Yoon J (2018) A new kind of rhodamine-based fluorescence turn-on probe for monitoring ATP in mitochondria. Sensors Actuators B Chem 265: 429–434

9. Wu WL, Zhao X, Xi LL, Huang MF, Zeng WH, Miao JY, Zhao BX (2017) A mitochondria-targeted fluorescence probe for ratiometric detection of endogenous hypochlorite in the living cells. Anal Chim Acta 950:178–183
10. Goswami S, Manna A, Paul S, Kheng Quah C, Fun HK (2013) Rapid and ratiometric detection of hypochlorite with real application in tap water: molecules to low cost devices (TLC sticks). Chem Commun 49:11656–11658
11. Yuan L, Lin W, Song J, Yang Y (2011) Development of an ICT-based ratiometric fluorescent hypochlorite probe suitable for living cell imaging. Chem Commun 47:12691–12693
12. Fukuzaki S (2006) Mechanisms of actions of sodium hypochlorite in cleaning and disinfection processes. Biocontrol Sci 11:147–157
13. Hou JT, Li K, Yang J, Yu KK, Liao YX, Ran YZ, Liu YH, Zhou XD, Yu XQ (2015) Ratiometric fluorescent probe for in situ quantification of basal mitochondrial hypochlorite in cancer cells. Chem Commun 51:6781–6784
14. Das S, Aich K, Patra L, Ghoshal K, Gharami S, Bhattacharyya M, Mondal TK (2018) Development of a new fluorescence ratiometric switch for endogenous hypochlorite detection in monocytes of diabetic subjects by dye release method. Tetrahedron Lett 59:1130–1135
15. Hawkins CL, Pattison DI, Davies MJ (2003) Hypochlorite-induced oxidation of amino acids, peptides and proteins. Amino Acids 25: 259–274
16. Wang X, Song F, Peng X (2016) A versatile fluorescent probe for imaging viscosity and hypochlorite in living cells. Dyes Pigments 125:89–94
17. Jiang Y, Wu S, Jin C, Wang B, Shen J (2018) Novel diaminomaleonitrile-based fluorescent probe for ratiometric detection and bioimaging of hypochlorite. Sensors Actuators B Chem 265:365–370
18. Zhao Y, Li H, Xue Y, Ren Y, Han T (2017) A phenanthroimidazole-based fluorescent probe for hypochlorous acid with high selectivity and its bio-imaging in living cells. Sensors Actuators B Chem 241: 335–341
19. Guo J, Zhang Z, Kuai Z, Wang R, Yang Q, Shan Y, Li Y (2017) A new turn-on fluorescent probe towards hypochlorite in living cells. Anal Methods 9:864–870
20. Goswami S, Aich K, Das S, Pakhira B, Ghoshal K, Quah CK, Bhattacharyya M, Fun HK, Sarkar S (2015) A triphenyl amine-based solvatofluorochromic dye for the selective and ratiometric sensing of OCl^- in human blood cells. Chem Asian J 10:694–700
21. Chen S, Lu J, Sun C, Ma H (2010) A highly specific ferrocene-based fluorescent probe for hypochlorous acid and its application to cell imaging. Analyst 135:577–582
22. Goswami S, Paul S, Manna A (2013) Highly reactive (<1 min) ratiometric "naked eye" detection of hypochlorite with real application in tap water. Dalton Trans 42:10097–10101
23. Sasikumar T, Ilanchelian M (2017) Colorimetric detection of hypochlorite based on the morphological changes of silver nanoprisms to spherical nanoparticles. Anal Methods 9:3151–3158
24. Choi MG, Ryu H, Cho MJ, Lee SK, Chang SK (2017) Dual signaling of hypochlorite in tap water by selective oxidation of phenylselenylated dichlorofluorescein. Sensors Actuators B Chem 244:307–313
25. Xiong K, Yin C, Chao J, Zhang Y, Huo F (2016) The detection for hypochlorite by UV–vis and fluorescent spectra based on oxidized ring opening and successive hydrolysis reaction. Spectrochim Acta A Mol Biomol Spectrosc 166:79–83
26. Ding S, Zhang Q, Xue S, Feng G (2015) Real-time detection of hypochlorite in tap water and biological samples by a colorimetric, ratiometric and near-infrared fluorescent turn-on probe. Analyst 140:4687–4693
27. Zhu B, Wu L, Zhang M, Wang Y, Liu C, Wang Z, Duan Q, Jia P (2018) A highly specific and ultrasensitive near-infrared fluorescent probe for imaging basal hypochlorite in the mitochondria of living cells. Biosens Bioelectron 107:218–223
28. Cheng X, Qu S, Zhong Z, Li W (2017) Coumarin-based fluorescent probe for Hypochlorites and real application in tap water. J Fluoresc 27:1427–1433
29. Wang Y, Xia J, Han J, Bao X, Li Y, Tang X, Ni L, Wang L, Gao M (2016) A fast-responsive fluorescent probe based on BODIPY dye for sensitive detection of hypochlorite and its application in real water samples. Talanta 161:847–853
30. Hu Q, Qin C, Huang L, Wang H, Liu Q, Zeng L (2018) Selective visualization of hypochlorite and its fluctuation in cancer cells by a mitochondria-targeting ratiometric fluorescent probe. Dyes Pigments 149:253–260
31. Zhang Y, Ma L, Tang C, Pan S, Shi D, Wang S, Li M, Guo Y (2018) A highly sensitive and rapidly responding fluorescent probe based on a rhodol fluorophore for imaging endogenous hypochlorite in living mice. J Mater Chem B 6:725–731
32. Vedamalai M, Kedaria D, Vasita R, Gupta I (2018) Oxidation of phenothiazine based fluorescent probe for hypochlorite and its application to live cell imaging. Sensors Actuators B Chem 263:137–142
33. Chen P, Zheng Z, Zhu Y, Dong Y, Wang F, Liang G (2017) Bioluminescent turn-on probe for sensing hypochlorite in vitro and in tumors. Anal Chem 89:5693–5696
34. Wang X, Wang X, Feng Y, Zhu M, Yin H, Guo Q, Meng X (2015) A two-photon fluorescent probe for detecting endogenous hypochlorite in living cells. Dalton Trans 44:6613–6619
35. Thiruppathi M, Thiyagarajan N, Gopinathan M, Chang JL, Zen JM (2017) A dually functional 4-aminophenylboronic acid dimer for voltammetric detection of hypochlorite, glucose and fructose. Microchim Acta 184:4073–4080
36. Li G, Lin Q, Sun L, Feng C, Zhang P, Yu B, Chen Y, Wen Y, Wang H, Ji L, Chao H (2015) A mitochondrial targeted two-photon iridium(III) phosphorescent probe for selective detection of hypochlorite in live cells and in vivo. Biomaterials 53:285–295
37. Wu Y, Wang J, Zeng F, Huang S, Huang J, Xie H, Yu C, Wu S (2016) Pyrene derivative emitting red or near-infrared light with monomer/excimer conversion and its application to Ratiometric detection of hypochlorite. ACS Appl Mater Interfaces 8:1511–1519
38. Chang C, Wang F, Qiang J, Zhang Z, Chen Y, Zhang W, Wang Y, Chen X (2017) Benzothiazole-based fluorescent sensor for hypochlorite detection and its application for biological imaging. Sensors Actuators B Chem 243:22–28
39. Qiao L, Nie H, Wu Y, Xin F, Gao C, Jing J, Zhang X (2017) An ultrafast responsive BODIPY-based fluorescent probe for the detection of endogenous hypochlorite in live cells. J Mater Chem B 5: 525–530
40. Xiao H, Xin K, Dou H, Yin G, Quan Y, Wang R (2015) A fast-responsive mitochondria-targeted fluorescent probe detecting endogenous hypochlorite in living RAW 264.7 cells and nude mouse. Chem Commun 51:1442–1445
41. Zang L, Liang C, Wang Y, Bu W, Sun H, Jiang S (2015) A highly specific pyrene-based fluorescent probe for hypochlorite and its application in cell imaging. Sensors Actuators B Chem 211:164–169
42. Gong H, Jiang Y, Hou RC, Ding XQ (2016) A sensitive and selective fluorescent coumarin-based probe for detection of hypochlorite ion and its application to cellular imaging. J Fluoresc 26:403–406
43. Fan J, Mu H, Zhu H, Wang J, Peng X (2015) Light up ClO^- in live cells using and aza-coumarin based fluorescent probe with fast response and high sesitivity. Analyst 140:4594–4598
44. Frisch MJ, Trucks GW, Schlegel HB, Scuseria GE, Robb MA, Cheeseman JR, Jr JAM, Vreven T, Kudin KN, Burant JC, Millam JM, Iyengar SS, Tomasi J, Barone V, Mennucci B, Cossi M, Scalmani G, Rega N, Petersson GA, Nakatsuji H, Hada M, Ehara M, Toyota K, Fukuda R, Hasegawa J, Ishida M, Nakajima T, Honda Y, Kitao O, Nakai H, Klene M, Li X, Knox JE, Hratchian HP, Cross JB, Bakken V, Adamo C, Jaramillo J, Gomperts R, Stratmann RE, Yazyev O,

Austin AJ, Cammi R, Pomelli C, Ochterski JW, Ayala PY, Morokuma K, Voth GA, Salvador P, Dannenberg JJ, Zakrzewski VG, Dapprich S, Daniels AD, Strain MC, Farkas O, Malick DK, Rabuck AD, Raghavachari K, Foresman, JJB, Ortiz V, Cui Q, Baboul AG, Clifford S, Cioslowski J, Stefanov BB, Liu G, Liashenko A, Piskorz P, Komaromi I, Martin RL, Fox DJ, Keith T, Al-Laham MA, Peng CY, Nanayakkara A, Challacombe M, Gill PMW, Johnson B, Chen W, Wong MW, Gonzalez C, Pople JA (2004) GAUSSIAN 03 (Revision B.02). Gaussian, Inc., Wallingford CT

45. Becke AD (1993) Density-functional thermochemistry. II. The role of exact exchang. J Chem Phys 98:5648–5652
46. Lee C, Yang W, Parr RG (1988) Development of the Colle-Salvetti correlation-energy formula into a functional of the electron density. Phys Rev B 37:785–789
47. Hariharan PC, Pople JA (1973) The influence of polarization functions on molecular orbital hydrogenation energies. Theor Chim Acta 28:213–222
48. Francl MM, Pietro WJ, Hehre WJ, Binkley JS, Gordon MS, DeFrees DJ, Pople JA (1982) Self-consistent molecular orbital methods. 23. A polarization-type basis set for 2nd-row elements. J Chem Phys 77:3654–3665
49. Barone V, Cossi M (1998) Quantum calculation of molecular energies and energy gradients in solution by a conductor solvent model. J Phys Chem 102:1995–2001
50. Cossi M, Barone V (2001) Time-dependent density functional theory for molecules in liquid solutions. J Chem Phys 115: 4708–4717
51. Yanai T, Tew DP, Handy NC (2004) A new hybrid exchange-correlation functional using the coulomb-attenuating method (CAM-B3LYP). Chem Phys Lett 393:51–57
52. O'boyle NM, Tenderholt AL, Langner KM (2008) Cclib: a library for package-independent computational chemistry algorithms. J Comput Chem 29:839–845
53. Tsui YK, Devaraj S, Yen YP (2012) Azo dyes featuring with nitrobenzoxadiazole (NBD) unit: a new selective chromogenic and fluorogenic sensor for cyanide ion. Sensors Actuators B Chem 161:510–519
54. Yang Y, Gao CY, Chen J, Zhang N, Dong D (2016) A pyrene-based fluorescent and colorimetric chemodosimeter for the detection of ClO^- ions. Anal Methods 8:805–809
55. Goswami S, Maity S, Maity AC, Das AK (2014) Fluorometric and naked-eye detectable dual signaling chemodosimeter for hypochlorite. Sensors Actuators B Chem 204:741–745